SAFETY ANALYSIS OF THE MOLTEN SALT FAST REACTOR FUEL COMPOSITION USING MOLTRES

(Preprint submitted to ANS Global 2019 International Fuel Cycle Conference)

Sun Myung Park[a,b], Andrei Rykhlevskii[a], and Kathryn D. Huff[a]

[a]*Dept. of Nuclear, Plasma and Radiological Engineering, University of Illinois at Urbana-Champaign*
[b]*smpark3@illinois.edu*

ABSTRACT

The Molten Salt Fast Reactor (MSFR) has garnered much interest for its inherent safety and sustainbility features. The MSFR can adopt a closed thorium fuel cycle for sustainable operation through the breeding of ^{233}U from ^{232}Th. The fuel composition changes significantly over the course of its lifespan. In this study, we investigated the steady state and transient behavior of the MSFR using Moltres, a coupled neutronics/thermal-hydraulics code developed within the Multiphysics Object Oriented Simulation Environment (MOOSE) framework. Three different fuel compositions, start-up, early-life, and equilibrium, were examined for potentially dangerous core temperature excursions during a unprotected loss of heat sink (ULOHS) accident. The six-group and total neutron flux distributions showed good agreement with SERPENT and published MSFR results, while the temperature distribution and total power showed discrepancies which can be attributed to known sources of error. For the transient behavior under the ULOHS scenario, while the transition time towards the new steady state core temperature is also in good agreement with existing MSFR simulations by Fiorina et al., Moltres underestimated the temperature rise by a factor of ten, due to the same sources of error affecting the steady state results. While an MSFR loaded with start-up fuel composition operates at a higher temperature than with the other two fuel compositions, all three cases were shown to be inherently safe due to the strong negative temperature feedback.

I INTRODUCTION

Molten Salt Reactors (MSRs) are a class of nuclear reactors that contain nuclear fuel dissolved and circulating in a molten salt coolant loop. They potentially possess the ability to run for extended periods with minimal shutdown time due to online fuel reprocessing. Their equilibrium fuel compositions differ substantially from start-up compositions not only due to burnup of initial fissile material and breeding of new fissile material, but also fissile material feeds and removal of fission products. Also, while early-life fuel composition is largely dependent on the initial core loading, the long-term equilibrium fuel composition is determined by the type of feed. Since the changing fuel composition impacts safety parameters (e.g. reactivity feedback coefficients), a licensing case for this class of reactors must fully characterize those impacts.

While numerous computational tools exist for conventional nuclear reactors, MSRs present unique computational challenges that many fail to address effectively. MSRs differ profoundly from conventional solid-fuelled reactors, particularly in their neutronics and thermal-hydraulics behaviors. New MSR simulation tools must capture strong coupling between neutronics and thermal-hydraulics exhibited by delayed neutron precursor (DNP) movement as well as strong Doppler and density feedback in the fuel salt. This paper investigates the impact of changing fuel composition on fuel salt temperatures in the Molten Salt Fast Reactor (MSFR) concept using a new simulation tool for MSRs, Moltres [1].

Moltres is an open source coupled neutronics/thermal hydraulics simulation application for simulating MSRs. Built on the Multiphysics Object-Oriented Simulation Environment (MOOSE) finite element framework [2], Moltres solves the coupled time-dependent multi-group neutron diffusion, temperature, and DNP governing equations. The temperature and DNP equations fully account for flow via fuel salt advection.

The MSFR model studied in this paper is a reference design for a fast-spectrum MSR developed under H2020 Safety Assessment of the Molten Salt Fast Reactor (SAMOFAR) project [3]. The MSFR boasts several safety and sustainability advantages over conventional reactors. Firstly, it can run on a closed thorium fuel cycle, which reduces actinide production and waste radiotoxity. The fast neutron spectrum improves ^{233}U breeding from ^{232}Th, an isotope that is approximately three times as abundant as uranium. Lastly, the MSFR operates at near atmospheric pressure; this reduces the risk of containment structure failure and manufacturing costs.

This paper presents results from Moltres simulations of the MSFR reference model with three fuel compositions: start-up, early-life, and equilibrium. In line with the purpose of the MSFR as a thorium breeder, the chosen start-up fuel composition under study is a eutectic mixture of ^{233}U and ^{232}Th fluorides in a lithium fluoride molten salt, with a Th/^{233}U mixture feed. ^{233}U is extracted from the blanket tank and reinserted into the core [4].

We generated group constants for each fuel composition using SERPENT [5], a continuous-energy Monte Carlo code for numerous reactor physics applications. The group constants relevant for Moltres simulations are the various macroscopic neutron cross sections, neutron diffusion coefficient, average fission energy, average neutron yield, inverse neutron speed, fission spectrum, DNP decay constants, and effective delayed neutron fractions. Using these group constants, Moltres then solves for the flux and temperature based on the neutron diffusion equation coupled with temperature advection due to coolant flow. Transient simulations will establish core fuel temperatures during transients. These distributions will give insight into MSFR transient behavior, which will help us identify potential safety risks.

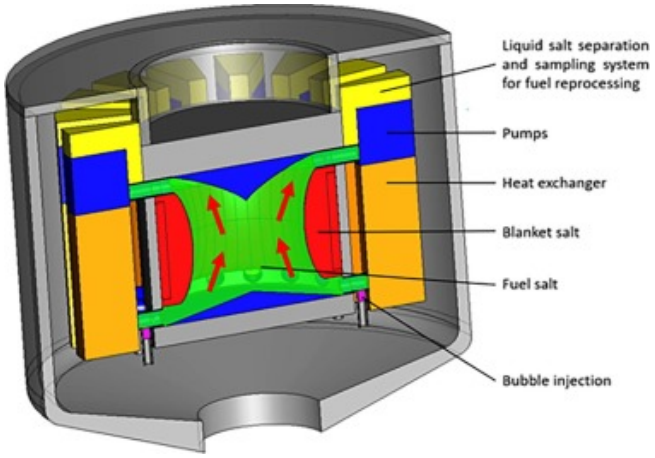

Fig. 1: MSFR reactor design concept [6].

TABLE I: Specifications of the MSFR design [6].

Parameter	Value
Thermal/Electric output [MW_{th}/MW_e]	3000 / 1500
Salt volume [m^3]	18
Salt fraction in core	0.5
Number of circulation loops	16
Nominal flow rate [kg s^{-1}]	18500
Nominal circulation time [s]	4.0
Inlet/outlet temperature [K]	923 / 1023
Blanket volume [m^3]	7.3

Section II provides the specifications and a literature review of the MSFR concept. Section III covers the overall modeling approach with respect to the codes used in this study: SERPENT and Moltres. Section IV presents steady state neutron flux and temperature distribution results from Moltres for the three different fuel compositions studied. Section V explores the MSFR's neutronic and thermodynamic response to a Unprotected Loss of Heat Sink (ULOHS) scenario. Lastly, Section VI provides conclusions and suggestions for future work.

II MOLTEN SALT FAST REACTOR

Figure 1 shows a schematic view of the MSFR. The main specifications of the MSFR are given in Table I.

Lithium fluoride (LiF) is the major component of the fuel and blanket molten salts used for the MSFR. Fissile and fertile isotopes are introduced into the mixture by mole fractions of 77.5%LiF-22.5%AcF_4, where AcF_4 represents actinide fluorides such as uranium and thorium fluorides. Table II shows the mole fraction of the molecular constituents in the MSFR fuel salt, with the relevant physical properties in Table III. The MSFR supports various fuel compositions; it can run on the same ^{235}U-^{238}U fuel used in most conventional LWRs. It can also run on a mixture of fresh and used uranium fuel containing reprocessed TRU isotopes [7]. However, the main configuration of the MSFR is a breeder reactor running on ^{233}U-^{232}Th [4]. Previous studies have reported breeding ratios of up to 1.1 on the MSFR [8].

TABLE II: Fuel salt composition used for the Serpent simulation.

Isotope	Mole fraction [%]
^{7}Li	29.0
^{19}F	62.6
^{232}Th	7.40
^{233}U	1.00

TABLE III: Fuel and blanket salt properties. T denotes temperature in Kelvins.

Property	Value
Density, ρ [kg m^{-3}]	$4983.56 - 0.882 \cdot T$
Thermal cond. , k [W m^{-1} K^{-1}]	$0.928 + 8.397 \times 10^{-5} \cdot T$
Specific heat, c_p [J kg^{-1} K^{-1}]	$-1111 + 2.78 \cdot T$

TABLE IV: Material compositions and densities of the absorber, and reflector regions. All elements listed are in their natural compositions.

Region	Element	At%	Density [kg m^{-3}]
Absorber	B	80	2520
	C	20	
Reflector	Ni	67.7	10000
	W	25.0	
	Cr	7.0	
	Al	0.3	

The primary fuel salt flows upwards through the 9 m^3 central core region. At the top of the core, the flow separates into 16 smaller external loops, each of which passes through a heat exchanger and is pumped back into the core. The primary heat exchangers transfer heat from the fuel salt to an intermediate salt coolant loop. There is other instrumentation along the external loops for online reprocessing and gas sparging. The core is radially surrounded by a tank of blanket molten salt, with reflectors at the top and bottom of the core. The blanket salt contains fertile isotopes such as ^{232}Th for fuel breeding. There is a layer of neutron absorbing material behind the blanket tanks to protect the heat exchangers, pumps and other instrumentation from neutron irradiation damage.

Various authors have performed a number of steady state and transient multiphysics simulations for the MSFR. A paper by Fiorina et al. [9] compares results between models developed on the multiphysics software COMSOL, and coupled in-house codes developed at Delft University of Technology. The models used 2D axisymmetric models of the MSFR and solved multi-group neutron diffusion equations for the neutronics, and they showed good agreement for some of the transient cases studied. A more comprehensive 3D model has been developed and studied by Aufiero et al. [10] using

the computional fluid dynamics (CFD) toolbox OpenFOAM. Although this model relied on the one group neutron diffusion equation, it enabled the study of the full 3D core geometry and 3D transient scenarios such as the failure of one of the 16 pumps in the MSFR.

More recently, a coupled tool, comprising of the thermal-hydraulics code TRACE and a multi-group 3D spatial neutronics solver Purdue Advanced Reactor Core Simulator (PARCS), was used to run steady state and transient simulations of the MSFR [11]. As PARCS only supports conventional fuel assembly shapes, the authors approximated the 3D axisymmetric cylindrical MSFR model with hexagonal fuel assemblies. This approach allowed for a 3D model simulation of the MSFR on a coarse mesh and showed good agreement with the COMSOL and TUDelft models with the benefit of much lower computation times in comparison to the OpenFOAM CFD model. On top of steady state simulations, the transient scenarios studied by Pettersen include loss of heat sink, pump over-speed, over-cooling and loss of flow.

As Moltres is developed on the MOOSE framework, it can perform implicit multiphysics coupling on an adaptive meshing scheme over multiple processing units for accurate and efficient MSR simulations. This paper aims to present Moltres simulation results and safety analysis of the MSFR, for various fuel compositions through its operational lifetime.

III METHODOLOGY

This section describes the overall modelling approach and the codes used in this paper. First, the early-life and equilibrium compositions were obtained from SCALE/TRITON unit cell depletion calculations by Rykhlevskii et al. [12] The authors used unit cell approximations for the modeling fuel cycle performance of the MSFR and three other fast-spectrum MSRs. We selected the equilibrium composition at approximately 43 years after start-up because the TRU vector change between each depletion time-step from this moment onwards is less than 3% [12]. For the early-life composition, it is the resulting fuel composition at 300 days after start-up.

We performed neutronics calculations on SERPENT using these fuel compositions and a truncated, reference MSFR core model [11] to generate six-group neutronics data for Moltres. The material compositions and densities for the absorber, and reflector regions are given in Table IV. We set a neutron population of 200,000 with 50 inactive cycles and 500 active cycles. For simplicity, the heat exchanger and pump region were modeled after Hastelloy N [13]. Isotopes in the fuel compositions, whose neutron cross-section data are not found in the JEFF-3.1.2 nuclear data library, were omitted from these calculations The energy boundaries for the six neutron groups were adopted from previous MSFR studies and shown in Table V. As for the DNP, there are eight DNP groups implicitly defined by the JEFF-3.1.2 nuclear data library. The reactor model is a 2D axisymmetric model as shown in Figure 2. This geometry focuses on the active central region of the core. Basing the geometry on the reference model facilitates comparisons with previous MSFR studies by various authors [9] [11] on the reference model for code-to-code verification purposes. The 2D model is extended into a 3D model in SERPENT by rotating it around the central axis to form concentric cylinders. Table VI shows the overall temperature reactivity feedback coefficients due to the Doppler effect and temperature-driven fuel salt expansion. The coefficients were derived by applying a least squares best fit on the multiplication factors at temperatures from 900 K to 1200 K with 50 K intervals.

TABLE V: Neutron energy group upper bounds used in Serpent.

Group number	Upper bound [MeV]
1	7.485×10^{-4}
2	5.5308×10^{-3}
3	$2.478\,75\times10^{-2}$
4	0.4979
5	2.2313
6	12

TABLE VI: Temperature reactivity feedback coefficients.

Composition	α_T [pcm K^{-1}]
Start-up	-7.39 ± 0.03
Early-life	-7.25 ± 0.03
Equilibrium	-6.24 ± 0.03

Finally, with the group constant data from SERPENT, Moltres calculated the resulting coupled neutron spectrum and temperature distribution for a given velocity profile in the core, from user-specified initial conditions towards steady state, or from steady state in the case of an accident scenario. We firther simplified the mesh geometry for Moltres from the SERPENT model by omitting the absorber, heat exchanger, and reflector regions. This is justified as they have negligible contribution towards the neutronics. Instead, a vacuum boundary condition was imposed on the outer surface of the blanket region, along with 923 K Dirichlet boundary conditions for temperature. The 2 cm thick blanket tank structural material was also omitted as its inclusion resulted in an extra fine mesh which drastically increased computational time. Figure 3 shows the Moltres MSFR mesh.

Moltres has a salt loop modeling capability to account for the flow and decay of DNPs outside the active core region. Moltres applies DNP boundary conditions at the inlets and outlets of the core and outer loop, determined by the inflow and outflow values of each DNP group at each time-step for each boundary. The DNP equations also govern the DNP behavior in the outer loop to allow for flow, production, and decay.

The velocity profile is a uniform velocity of 1.1275 ms^{-1} throughout the active core and outer loop regions. This value is derived from the MSFR loop circulation time of 4 s. Moltres also has heat exchanger modeling capabilities, represented in 3 by the heat sink term. For this paper, it is implemented at the midpoint of the outer loop region, with the heat loss value fixed to induce an approximately 100 K drop in temperature as specified by the MSFR design inlet/outlet temperature difference.

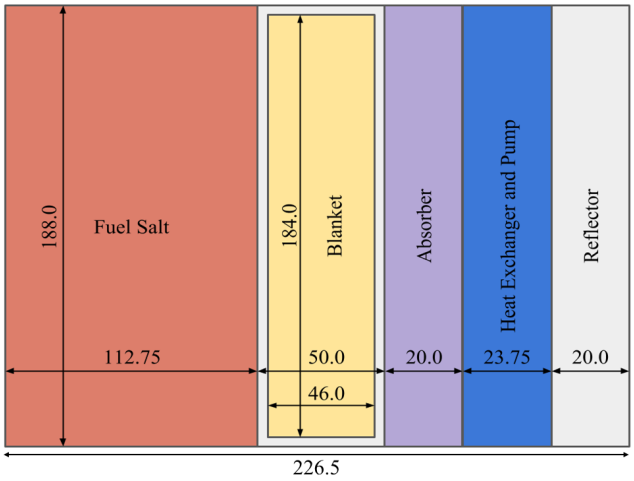

Fig. 2: Cross-section of the 2D axisymmetric model used in SERPENT. Derived from the MSFR reference model [11]. Figure is not drawn to scale. All dimensions are in cm.

III.A Moltres Code

This subsection provides the theoretical background for the coupled neutronics/thermal-hydraulics physics implemented in Moltres.

Moltres is an application code developed in the MOOSE framework [2]. MOOSE application codes solve non-linear problems through the discretization of partial differential equations (PDEs) on an adaptive coarse meshing scheme provided by LibMesh [14] and PetSc [15]. Individual terms of PDEs that define the physics involved in a system are represented in MOOSE (and its applications) by kernels. For example, the various terms in the neutron diffusion equation such as the diffusion term, time evolution term, etc. all have a corresponding physics kernel defined in Moltres. Boundary conditions are also handled in a similar fashion. Moltres can solve for an arbitrary number of neutronics groups as long as the relevant group constants are provided in a compatible text format.

As mentioned in the previous Moltres study [1], the neutronics in Moltres is described by the time-independent multi-group neutron diffusion equation as shown in Equation 1:

$$\frac{1}{v_g}\frac{\partial \phi_g}{\partial t} - \nabla \cdot D_g \nabla \phi_g + \Sigma_g^r \phi_g = \sum_{g \neq g'}^{G} \Sigma_{g' \to g}^s \phi_{g'} + \chi_g^p \sum_{g'=1}^{G} (1-\beta) \nu \Sigma_{g'}^f \phi_{g'} + \chi_g^d \sum_{i}^{I} \lambda_i C_i, \quad (1)$$

where

v_g = average speed of neutrons in group g
ϕ_g = flux of neutrons in group g
t = time
D_g = diffusion coefficient of neutrons in group g
Σ_g^r = macroscopic cross-section for removal of neutrons from group g
$\Sigma_{g' \to g}^s$ = macroscopic cross-section of scattering from g' to g
χ_g^p = prompt fission spectrum neutrons in group g
G = number of discrete neutron groups, g
ν = average number of neutrons produced per fission
Σ_g^f = macroscopic fission cross-section for neutron in group g
χ_g^d = delayed fission spectrum neutrons in group g
I = number of delayed neutron precursor groups
β = delayed neutron fraction
λ_i = average decay constant of delayed neutron precursors in precursor group i
C_i = concentration of delayed neutron precursors in precursor group i.

The DNPs are governed by the following equation:

$$\frac{\partial C_i}{\partial t} = \sum_{g'=1}^{G} \beta_i \nu \Sigma_{g'}^f \phi_{g'} - \lambda_i C_i - \frac{\partial}{\partial z} u C_i. \quad (2)$$

Lastly, the governing equation for temperature in the molten salt is given as:

$$\rho c_p \frac{\partial T}{\partial t} + \nabla \cdot (\rho c_p \vec{u} \cdot T - k \nabla T) = Q_s - Q_{hx}, \quad (3)$$

where

ρ = density of molten salt
c_p = specific heat capacity of molten salt
T = temperature of molten salt
$\vec{u}$ = velocity of molten salt
k = thermal conductivity of molten salt
Q_{hx} = heat sink,

and the source term Q_s is given as:

$$Q_s = \sum_{g=1}^{G} \epsilon_g \Sigma_g^f \phi_g. \quad (4)$$

IV STEADY STATE NEUTRON FLUX AND TEMPERATURE DISTRIBUTION

We first ran Moltres in steady-state solver mode to generate the six-group neutron flux distribution at a temperature of 973 K with the start-up fuel composition. This is verified against the six-group flux generated directly from SERPENT after collapsing the fine-group flux. Figure 4 shows the neutron flux distributions from SERPENT and Moltres, with precursor drift disabled for code verification. There is very good agreement between the six group flux distributions from SERPENT and Moltres.

Next, the MSFR Moltres simulations were run in transient mode, with adaptive time-stepping and an initial, uniform neutron flux of 10^{14} cm^{-2} s^{-1} and an initial temperature of 923

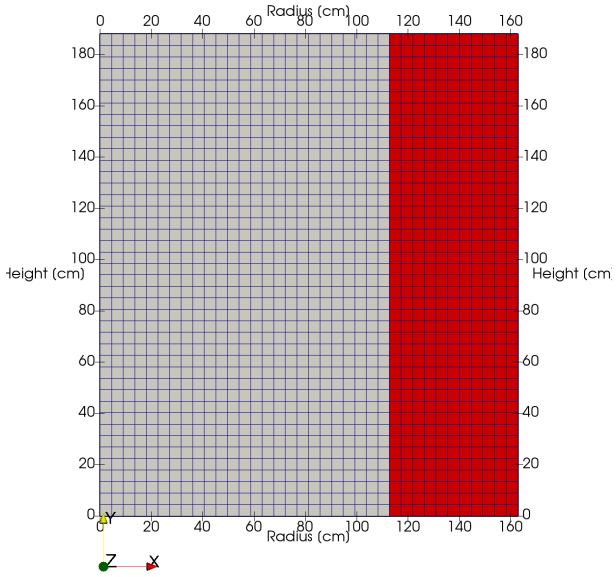

Fig. 3: Mesh of the 2D axisymmetric model used in Moltres. The grey and red regions represent the fuel and blanket salt respectively.

K throughout the fuel and blanket regions, for the start-up, early-life, and equilibrium fuel compositions. The simulations reached steady state after 100 s, as the volume-integrated neutron flux values varied by less than 0.001% over the previous ten seconds. The computational time for each case averages at 30 minutes when run on four processing units on a workstation.

Figure 5 shows the total radial neutron flux at reactor half-height, with the three fuel compositions at steady state. The peak neutron flux value is highest for the start-up composition, followed by the early-life and equilibrium compositions. All three values are slightly lower than the peak value of approximately 8.6×10^{15} cm^{-2} s^{-1} reported by Fiorina et al. [7]. This

TABLE VII: Average fuel inlet temperature.

Composition	Inlet temperature [K]
Start-up	964.85
Early-life	925.11
Equilibrium	916.85

TABLE VIII: Average fuel outlet temperature.

Composition	Outlet temperature [K]
Start-up	1067.40
Early-life	1025.39
Equilibrium	1016.67

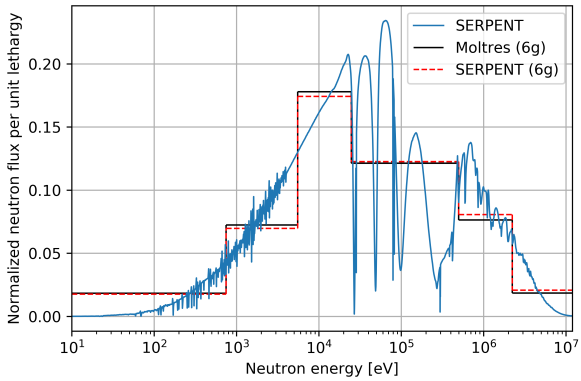

Fig. 4: Fine-group and six-group neutron flux distributions from SERPENT and Moltres.

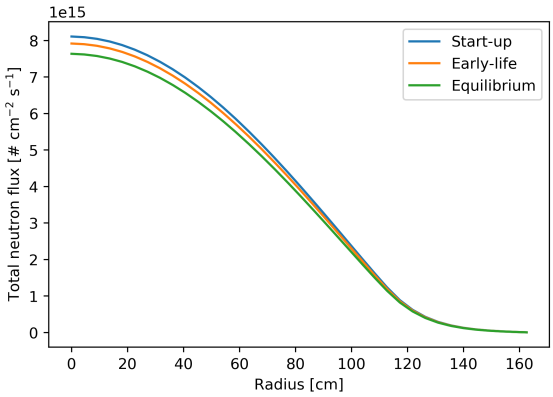

Fig. 5: Total radial neutron flux at reactor half-height, for start-up, early-life, and equilibrium fuel compositions at steady state.

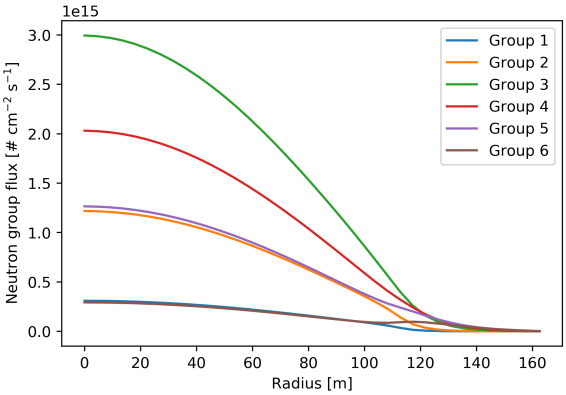

Fig. 6: Neutron group fluxes at reactor half-height, for start-up fuel composition at steady state.

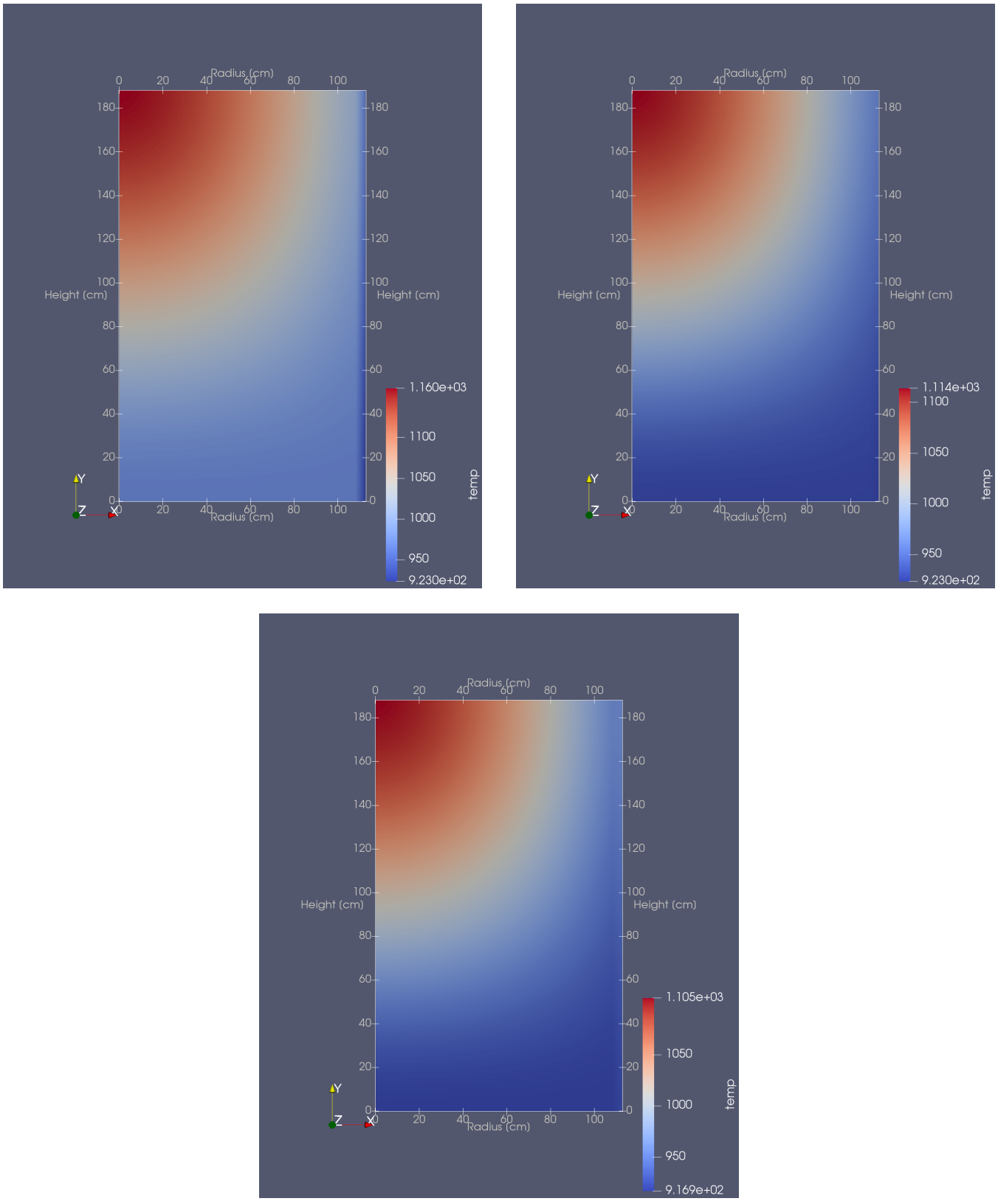

Fig. 7: Temperature distributions within the fuel salt region, for start-up (top left), early-life (top right), and equilibrium (bottom) fuel compositions at steady state. The height and radius are in the Y and X directions respectively.

may be due to the truncation of the top and bottom fuel regions of the core for the model used here. The vacuum boundary conditions were imposed closer to the center and resulted in a lower peak value. Figure 6 shows the six neutron group fluxes for the start-up fuel composition.

Heat transfer is dominated by advection as is observed by the temperature distributions in Figure 7. Given that flux is the highest at the center of the core, most of the heat is produced there. The upward flow pushes the temperature peak up to the outlet boundary. Tables VII and VIII show the average fuel inlet and outlet temperatures for the three cases.

The average outlet temperatures for all three compositions are close to the MSFR outlet temperature specification of 1023 K. Due to having a Reynolds number, significant mixing and heat transfer is expected in the fuel salt as it flows out of the core and through the outer loop. However, the center of the top reflector region is exposed to dangerously high peak temperatures of greater than 1100 K in all three cases as observed in Figure 7. In addition, higher temperatures are expected during dangerous accident scenarios.

In actuality, the peak temperatures are likely to be lower than the values seen in Figure 7 because of turbulent mixing. In choosing a uniform velocity profile, we have also implied that flow is laminar, which is a weak assumption given the high Reynolds number of molten salt flow in the MSFR. Turbulent temperature mixing could potentially be approximated by incorporating it into the conduction term as turbulent diffusion.

The uniform velocity approximation in our models also resulted in a significantly different spatial temperature distribution shape as compared to the results by Fiorina et al. [9] and Pettersen [11]. Their models feature significant flow stagnation in the fuel salt near the blanket tank. This causes their temperatures distributions to peak near the blanket tank as opposed to the center of the core as seen in Figure 7. However, improved models of the MSFR, as shown by Aufiero et al. [10], have temperature distributions closer to the results in this paper through curved walls that optimize salt flow.

Total power, as defined by Eq. 4, at steady state is approximately 2 GW. This is 1 GW less than the rated 3 GW of the MSFR. This may be mainly due to the erroneous uniform velocity profile imposed in the core. From fluid dynamics, velocity along the central axis of the core should be higher than the velocity at the periphral areas near the blanket tank. The higher velocity at the center results in higher advective heat transfer away from the center of the core and cools the active region. This should result in an increase in neutron flux from the strong negative temperature reactivity feedback, and thus higher heat generation. The truncation of the top and bottom fuel salt region is also a factor for the lower than expected heat production.

Comparing the three different fuel compositions, the MSFR operates at the highest temperatures with the start-up fuel composition, followed by the early-life, and the equilibrium compositions. This may be due to the generation of ^{233}Pa as an intermediate for ^{233}U breeding as mentioned by Rykhlevskii et al. [12] in their fuel cycle analysis of the MSFR; ^{233}Pa is a precursor for the ^{234}U neutron poison.

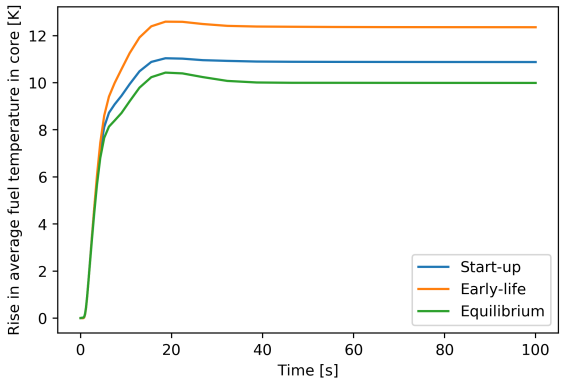

Fig. 8: Rise in average core fuel temperature for start-up, early-life, and equilibrium fuel compositions during ULOHS.

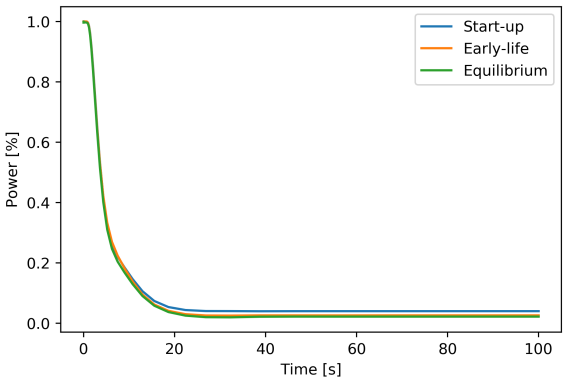

Fig. 9: Power generated, for start-up, early-life, and equilibrium fuel compositions during ULOHS.

V UNPROTECTED LOSS OF HEAT SINK

ULOHS may occur due to various causes of failure in the heat exchanger or secondary coolant loop such as secondary loop pump failure or loss of secondary coolant. While it is less likely in an MSFR as it consists of 16 separate coolant loops each with its own secondary cooling system, the potential consequences must still be studied. The loss of secondary cooling is simulated by exponentially decreasing the heat loss rate in the Moltres heat exchanger kernel with a time constant of 5 s.

ULOHS is expected to cause temperatures to increase, followed by a decrease in neutron flux and heat generation due to the strong negative temperature reactivity feedback. Eventually, the MSFR should settle on a new steady state with a higher average temperature than the operating temperature. If the high temperature is sustained for a long period of time, it could lead to severe damage in the reactor, pipes, or other instruments.

As observed in Figure 8, the average fuel temperature starts rising approximately 0.7 s after initiation. The MSFR reaches a new steady state approximately 10 K higher than the initial temperature after 30 s. While the transition time to

reach the new steady state is in good agreement with results reported by Fiorina et al. [9], the temperature rise is much smaller than the 100 K increase reported by the same authors. Power generation falls by two orders of magnitude (Figure 9), resulting in a negligible temperature difference between the inlets and outlets for all three fuel compositions. This could also be attributed to the relatively small total power of 2 GW discussed in the previous section, and the truncated MSFR model.

In comparing the three fuel compositions, an MSFR loaded with start-up fuel composition is at a higher safety risk as it has higher temperatures under normal operating conditions and accident scenarios.

VI CONCLUSION

In this study, we investigated the steady state, and transient behavior of the MSFR during a ULOHS using the coupled neutronics/thermal-hydraulics code Moltres. Moltres boasts relatively fast computational times due to a combination of parallelization, adaptive coarse meshing scheme and adaptive time-stepping. We verified the six-group neutron flux distribution at 973 K from Moltres against SERPENT. The total peak neutron flux at steady state agrees very closely with published results by Fiorina et al. [9].

While the temperature distribution and total power have large discrepancies, we have accounted for the main sources of error: the erroneous uniform velocity profile and the reactor model truncation. We also observed that the MSFR operates at a higher temperature with the start-up fuel composition than with the early-life and equilibrium compositions, due to the presence of ^{233}Pa. The high peak temperatures near the center of the top reflector are a potential safety risk. While this high temperatures could have been exacerbated by absence of turbulent diffusion implementation in Moltres, it warrants the need for further safety analysis.

During a ULOHS, the MSFR core fuel salt temperatures rise by approximately 10 K after a transition time of 30 s. While this time duration is similar to published results, the temperature rise is relatively low compared to the 100 K rise reported by Fiorina et al. [9] This discrepancy is also attributed to the same sources of error for the steady state results. Nonetheless, a temperature rise of this magnitude is relatively benign to reactor components, and makes a strong safety case for MSRs due to their strong negative temperature feedback, with the exception of the central top reflector region discussed previously.

Further development of the models is necessary to improve the accuracy and reliability of Moltres as a coupled neutronics/thermal-hydraulics code. Further work includes using an arbitrarily defined velocity profile, such as a parabolic profile. A better option would be the development of a Navier-Stokes module to generate an accurate velocity profile. A turbulent diffusion model would also be an essential addition to account for turbulent temperature mixing.

The heat exchanger functionality in Moltres can be improved beyond the current implementation of a fixed heat sink. The relevant heat transfer parameters between the primary and secondary loop in the heat exchanger would be necessary for a more complicated heat exchanger system.

ACKNOWLEDGEMENTS

The authors thank members of the Advanced Reactors and Fuel Cycles (ARFC) group at the University of Illinois at Urbana-Champaign for helpful discussions relating to this paper. Sun Myung Park is supported by the Singapore Nuclear Research and Safety Initiative (SNRSI) Postgraduate Scholarship.

REFERENCES

1. A. LINDSAY, G. RIDLEY, A. RYKHLEVSKII, and K. HUFF, "Introduction to Moltres: An application for simulation of Molten Salt Reactors," *Annals of Nuclear Energy*, **114**, 530–540 (Apr. 2018).
2. D. GASTON, C. NEWMAN, G. HANSEN, and D. LEBRUN-GRANDIE, "MOOSE: A parallel computational framework for coupled systems of nonlinear equations," *Nuclear Engineering and Design*, **239**, *10*, 1768–1778 (Oct. 2009).
3. D. GÃL'RARDIN, M. ALLIBERT, D. HEUER, A. LAUREAU, E. MERLE-LUCOTTE, and C. SEUVRE, "Design Evolutions of the Molten Salt Fast Reactor," p. 10.
4. E. MERLE-LUCOTTE, D. HEUER, M. ALLIBERT, M. BROVCHENKO, N. CAPELLAN, and V. GHETTA, "Launching the thorium fuel cycle with the Molten Salt Fast Reactor," in "Proceedings of ICAPP," (2011), pp. 2–5.
5. J. LEPPANEN, M. PUSA, T. VIITANEN, V. VALTAVIRTA, and T. KALTIAISENAHO, "The Serpent Monte Carlo code: Status, development and applications in 2013," *Annals of Nuclear Energy*, **82**, 142–150 (Aug. 2015).
6. J. SERP, M. ALLIBERT, O. BENES, S. DELPECH, O. FEYNBERG, V. GHETTA, D. HEUER, D. HOLCOMB, V. IGNATIEV, J. L. KLOOSTERMAN, L. LUZZI, E. MERLE-LUCOTTE, J. UHLÃŊÅŹ, R. YOSHIOKA, and D. ZHIMIN, "The molten salt reactor (MSR) in generation IV: Overview and perspectives," *Progress in Nuclear Energy*, **77**, *Supplement C*, 308–319 (Nov. 2014).
7. C. FIORINA, M. AUFIERO, A. CAMMI, F. FRANCESCHINI, J. KREPEL, L. LUZZI, K. MIKITYUK, and M. E. RICOTTI, "Investigation of the MSFR core physics and fuel cycle characteristics," *Progress in Nuclear Energy*, **68**, 153–168 (Sep. 2013).
8. C. FIORINA, *The molten salt fast reactor as a fast spectrum candidate for thorium implementation*, PhD, Politecnico Di Milano (Mar. 2013).
9. C. FIORINA, D. LATHOUWERS, M. AUFIERO, A. CAMMI, C. GUERRIERI, J. L. KLOOSTERMAN, L. LUZZI, and M. E. RICOTTI, "Modelling and analysis of the MSFR transient behaviour," *Annals of Nuclear Energy*, **64**, *Supplement C*, 485–498 (Feb. 2014).
10. M. AUFIERO, A. CAMMI, O. GEOFFROY, M. LOSA, L. LUZZI, M. E. RICOTTI, and H. ROUCH, "Development of an OpenFOAM model for the Molten Salt Fast Reactor transient analysis," *Chemical Engineering Science*, **111**, 390–401 (May 2014).

11. E. E. PETTERSEN and K. MIKITYUK, *Coupled multi-physics simulations of the Molten Salt Fast Reactor using coarse-mesh thermal-hydraulics and spatial neutronics*, Master's thesis, MSc thesis, September 2016 (PDF) (2016).
12. A. RYKHLEVSKII, B. BETZLER, A. WORRALL, and K. HUFF, "Fuel Cycle Performance of Fast Spectrum Molten Salt Reactor Designs," in "Int. Conf. Mathematics and Computational Methods Applied to Nuclear Science and Engineering," (2019).
13. "Hastelloy ® N alloy," Tech. rep., Haynes International (2017).
14. B. S. KIRK, J. W. PETERSON, R. H. STOGNER, and G. F. CAREY, "libMesh: a C++ library for parallel adaptive mesh refinement/coarsening simulations," *Engineering with Computers*, **22**, *3-4*, 237–254 (Dec. 2006).
15. SATISH BALAY, SHRIRANG ABHYANKAR, MARK ADAMS, JED BROWN, PETER BRUNE, KRIS BUSCHELMAN, LISANDRO DALCIN, VICTOR EIJKHOUT, WILLIAM GROP, DINESH KAUSHIK, MATTHEW KNEPLEY, LOIS CURFMAN MCINNES, KARL RUPP, BARRY SMITH, STEFANO ZAMPINI, and HONG ZHANG, "PETSc Users Manual," Tech. Rep. ANL-95/11 - Revision 3.6, Argonne National Laboratory (2015).